PROCEEDINGS, Thirty-Eighth Workshop on Geothermal Reservoir Engineering
Stanford University, Stanford, California, February 11-13, 2013
SGP-TR-198

GEOLOGIC MODEL OF THE GEOTHERMAL ANOMALY AT PILGRIM HOT SPRINGS, SEWARD PENINSULA, ALASKA

Joshua K. Miller[1] , Dr. Anupma Prakash[2], Dr. Ronald Daanen[3], Dr. Christian Haselwimmer[4], Dr. Michael Whalen[5], Dick Benoit[6], William Cumming[7], Arthur C. Clark[8] , Markus Mager[9], Gwen Holdmann[10]

[1]Geophysical Institute, Univeristy of Alaska Fairbanks,
P.O. Box 750421, Fairbanks, AK, 99775, USA
jkmiller3@alaska.edu
(Author information listed in References)

ABSTRACT

Pilgrim Hot Springs has a known shallow geothermal reservoir with temperatures approaching 91˚C in the top 100 meters of the system that underlies the main hot springs area of 1.5 km^2. The deeper reservoir is less understood with similar temperatures at the basement surface 320 meters directly beneath the hot springs. The aspect of this research is to create a stratigraphic model and delineate potential flow paths for the upflow zone of the geothermal anomaly. Lithology, well logs, temperature data, and magnetotelluric survey maps indicate a shallow outflow aquifer at 50 meters depth, a low permeability clay cap at 200-275 meters depth above the deeper reservoir, and an upflow of 90°C geothermal fluids that correlates to an indurated zone to the basement surface. The geothermal fluids may be flowing from a fault in the bedrock in the center of the hot springs although the deeper source is speculative.

INTRODUCTION

The Pilgrim Hot Springs geothermal system (Fig. 1) is being investigated by the University of Alaska Fairbanks Geophysical Institute and the Alaska Center for Energy and Power. Exploration of this geothermal site has been conducted since 1979 and was the first to be extensively explored in Alaska. The goal of recent exploration is the development of the geothermal system to provide power or direct-use heating to nearby communities on the Seward Peninsula including the city of Nome.

Results from previous studies have concluded that the system is alkali-chloride rich and fluid-dominated with deeper reservoir temperature of 130°C (Turner et al., 1980). Two 50 m exploratory wells established a temperature gradient up to 90°C (Turner et al., 1980). In 1982, four tightly-spaced exploration wells were drilled up to depths of 350 m. The rate of flow of geothermal fluids from these wells was estimated at ~200 gpm. In the known geothermal area numerous springs discharge geothermal fluids at a

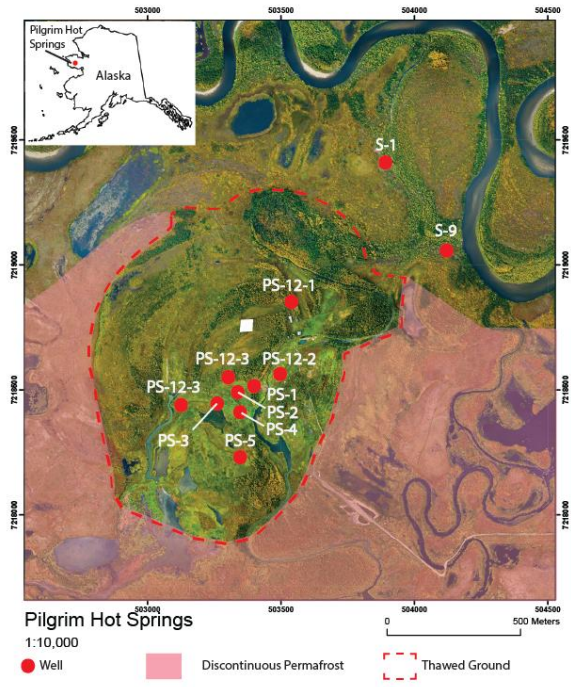

Figure 1. Location map of Pilgrim Hot Springs showing the distribution of wells, the boundary of discontinuous permafrost, and the extent of the thawed ground anomaly.

rate of 0.5 cfs. Spring water geochemistry suggests a higher, deeper reservoir temperature of 150° C (Lofgren, 1983). Beginning in 2010, the Alaska Center for Energy and Power and the Geophysical Institute of the University of Alaska Fairbanks are now testing the application of forward looking infrared radiometry (FLIR) remote sensing to reduce the cost of preliminary geothermal exploration by surveying elevated heat loss at the surface of Pilgrim Hot Springs (Daanen et al., 2012; Haselwimmer et al., 2011). Exploration drilling based on the FLIR survey results has produced five slimhole wells, 50+ shallow Geoprobe temperature gradient holes, and a magnetotelluric (MT) resistivity ground survey.

REGIONAL GEOLOGY

Pilgrim Hot Springs is located on the Seward Peninsula in western Alaska, less than 200 km south of the Arctic Circle. The springs are within an alluvial basin bounded by the glacially-eroded Kigluaik Mountains to the south and two prominent hills to the north, Marys Mountain and the Hen and Chicken Mountains. The basin is dissected by the east to west meandering Pilgrim River that borders the thawed ground of the springs, which occupies an ~ 1.5 km^2 area (Fig. 1). The thawed ground is associated with anomalous vegetation that includes cottonwood trees, alders, grass, and various flowers. The site lies only a few meters above sea level and elevation changes are small. The surficial and bedrock geology of the study area is summarized in Figure 2 that has been updated from the work of Turner et al. (1979) and Till et al. (2011). The surface expression of bedrock is only apparent in the nearby mountains as the valley is mostly thermokarst lakes, tundra underlain with permafrost, and muskeg swamps. The composition of the basement block underlying the springs is described as Late Proterozoic amphibolite to granulite facies metamorphic rock. Outcrops of the metamorphic rocks occur in decreasing metamorphic grade to the

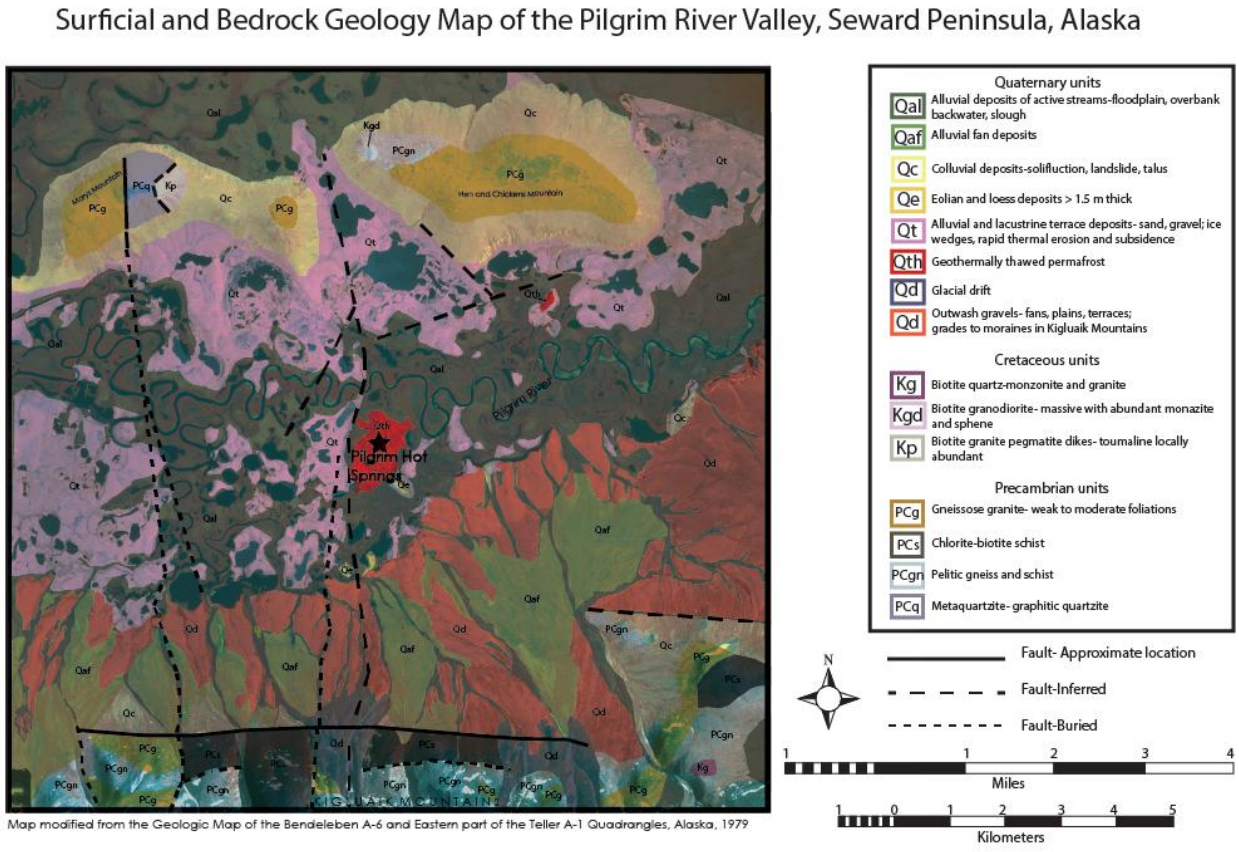

Figure 2. The surficial and bedrock geology map of the Pilgrim River Valley, Seward Peninsula, Alaska, modified from Turner et al., 1979, showing the Quaternary, Cretaceous, and Precambrian units in the immediate area. Many surface deposits are the result of Quaternary glaciation and permafrost-related features.

outer flanks of the Kigluaik Mountains intruded by an undifferentiated Cretaceous granite and metagranite (Amato et al., 2004; Till et al., 2011). A large field of Cenozoic basalt lies 50 km NE from Pilgrim Hot Springs with evidence of volcanism as recent as a few thousand years (Till et al., 2011). The Kigluaik range-front fault at the northern base of the mountain has been previously determined and mapped as a normal fault in a strongly extensional setting (Ruppert et al., 2008; Turner et al., 1980).

LITHOLOGIC LOGS

Unconsolidated to poorly consolidated Quaternary alluvial, fluvial, glaciolacustrine, and brackish lagoon sediments ranging from clay to gravel were intercepted in the wells to depths of 320 m where the mica schist basement was encountered below. Characterization of the drill cuttings from each well were used to produce lithological logs that provide the framework for development of a conceptual geological model of the geothermal system. The sediment characterization also provides porosity and permeability values which are important as input parameters for the numerical reservoir model. The USGS Central Region Research Drilling Program provided drilling and well logging support. The descriptions characterized the sediments by distribution of grain size from clay, silt, very fine-coarse sand, and gravels (Fig. 3). RockWorks 15, a geologic modeling program from RockWare, was used to create the visual model to generate cross-sections and maps for data comparison.

In Figure 3, a SW-NE cross-section is used to demonstrate the stratigraphy of the underlying sediments. Coarse sand is the most common sediment type derived from the edge of the proximal alluvial apron. Several horizontal clay layers are evident and are most abundant in PS-12-1. The thickest and most extensive clay rich layer seems to be located between depths of 200-275 m, about 50 m above the buried

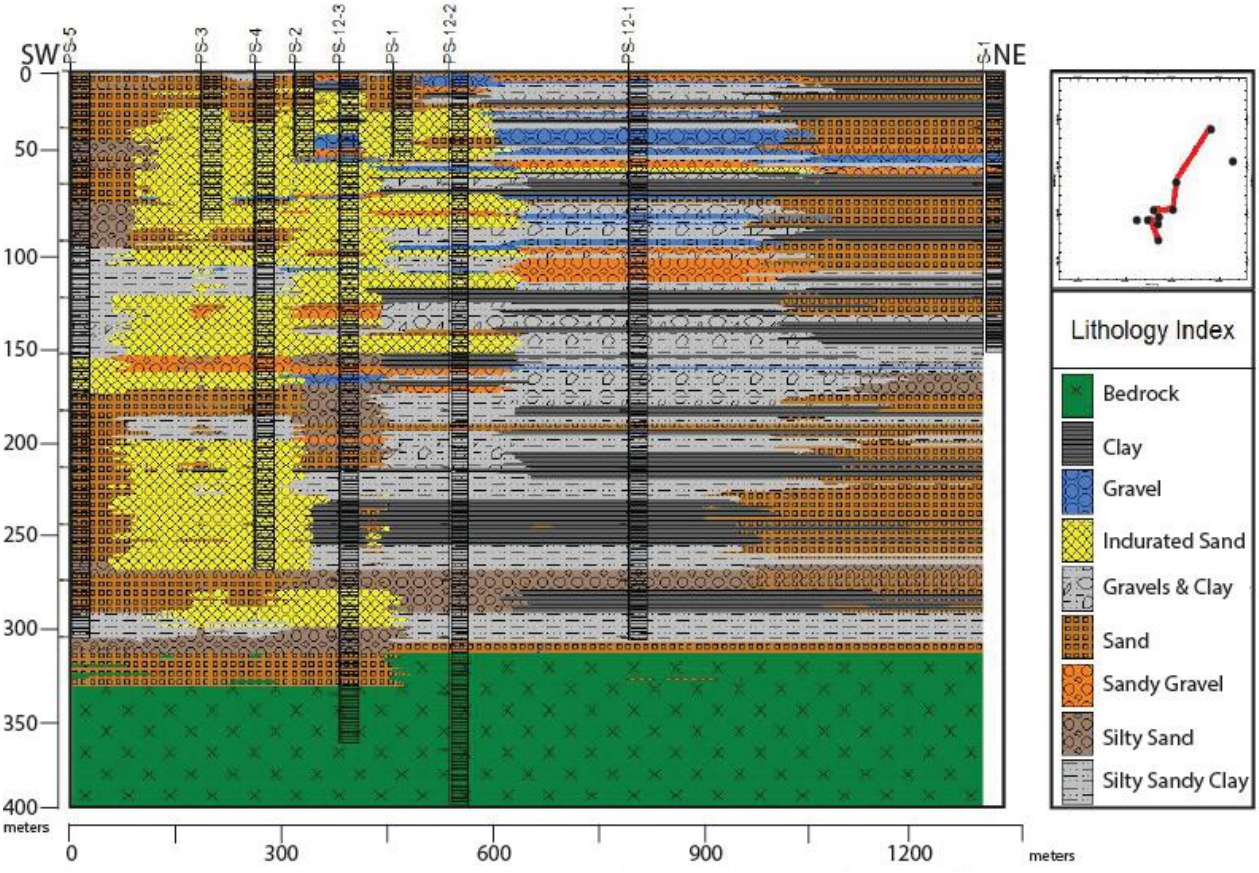

Figure 3. SW-NE cross-section from the RockWorks15 program showing the stratigraphic correlations between each lithologic column.

basement surface, and is intercepted in wells PS-12-1, PS-12-2, and PS-12-3. Another clay layer above the basement at ~300 m is present in all of the deep wells except PS-12-3. Beneath this clay is a zone of silty sand to the basement-sediment contact. A break or discontinuity in this clay at PS-12-3 has been replaced by indurated sand. There are other laterally extensive clay layers and are typically grey and silty-sandy. The lenses of gravel, most likely fluvial channel lag, have the highest primary porosity of the sediments and allow for the best communication of groundwater influx into the system. The gravels are typically thin and interbedded with clay or as distinct layers in the indurated zones.

Induration occurs in the subsurface to the basement with varying degrees of cementation. The indurated sediments have a clean silica cement and tend to be moderate to well-sorted sand. Penetration of these zones occurred in every well with the exception of S-1 and S-9. Induration seems to be greatest around PS-4 and forms a "chimney" with various lateral splays up section.

The composition of the basement is a mica schist that was determined from the lowermost ~20 m of core from the well PS-12-2. Aside from abundant pyrite mineral replacement, extensive hydrothermal alteration is not apparent although it has not been fully inspected. Basement was also intercepted in PS-12-3 with possible difference in depth. Due to the obliquity of the cross-section, the actual change in depth to basement between the two holes is less dramatic than Figure 3 indicates. The maximum difference is ~10 m where PS-12-3 is lower. If this is a small offset and not the effect of changing surface topography, this could be evidence of a fault at depth. However, the orientation and dip of the probable fault remains elusive.

TEMPERATURE AND GEOPHYSICAL LOGS

Borehole temperatures in Figure 4 were recorded using a Kuster K10 Strain Pressure/Temperature gauge. All temperatures were recorded at different time intervals of hours to weeks after drilling circulation ended to monitor temperature equilibration. Geophysical logs were also obtained for wells where entry or re-entry was possible. Below, lithologic, natural gamma ray, and temperature logs for several wells are provided for cross-comparison in Figure 5.

The temperature curves in Figure 4 show a spike in temperature up to 91°C at 25-50 m and subsequent reversal at 30-100 m. All wells show an increasing temperature gradient below the reversal of different rates. The shallow peak in temperature is the result of the outflow of geothermal fluids and the increasing temperature gradient is the heating of the deeper geothermal reservoir. It should be noted that the curve for PS-4 is not reliable below 140 m and the multiple fluctuations in PS-5's curve are equipment-related. These measurements were recorded during earlier exploration in the 1980's. Wells S-1 and S-9 seem to have only residual outflow fluids and a higher degree of mixing with meteoric groundwater water due to the low temperatures at the corresponding depth of peak outflow temperatures. The outflow aquifer temperature is highest in wells PS-12-2 and PS-12-3 which also have the highest bottom hole temperatures of 90°C and 80°C, respectively. The influx of groundwater is estimated to have a flow rate of ~200 gpm, as mentioned earlier, flowing through the system from the south to the north, eventually feeding into the Pilgrim River (Lofgren, 1983). The reversal from 30-100 m is attributed to a large degree of mixing with this colder meteoric water where permeability is sufficiently high.

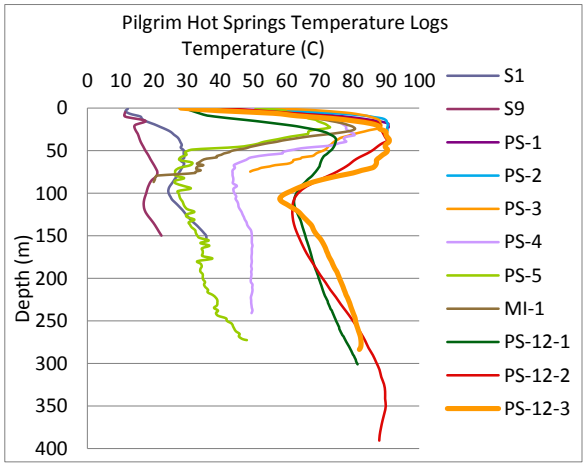

Figure 4. Temperature curves of each well at Pilgrim Hot Springs measured in degrees Celsius from 0-400 meter depth.

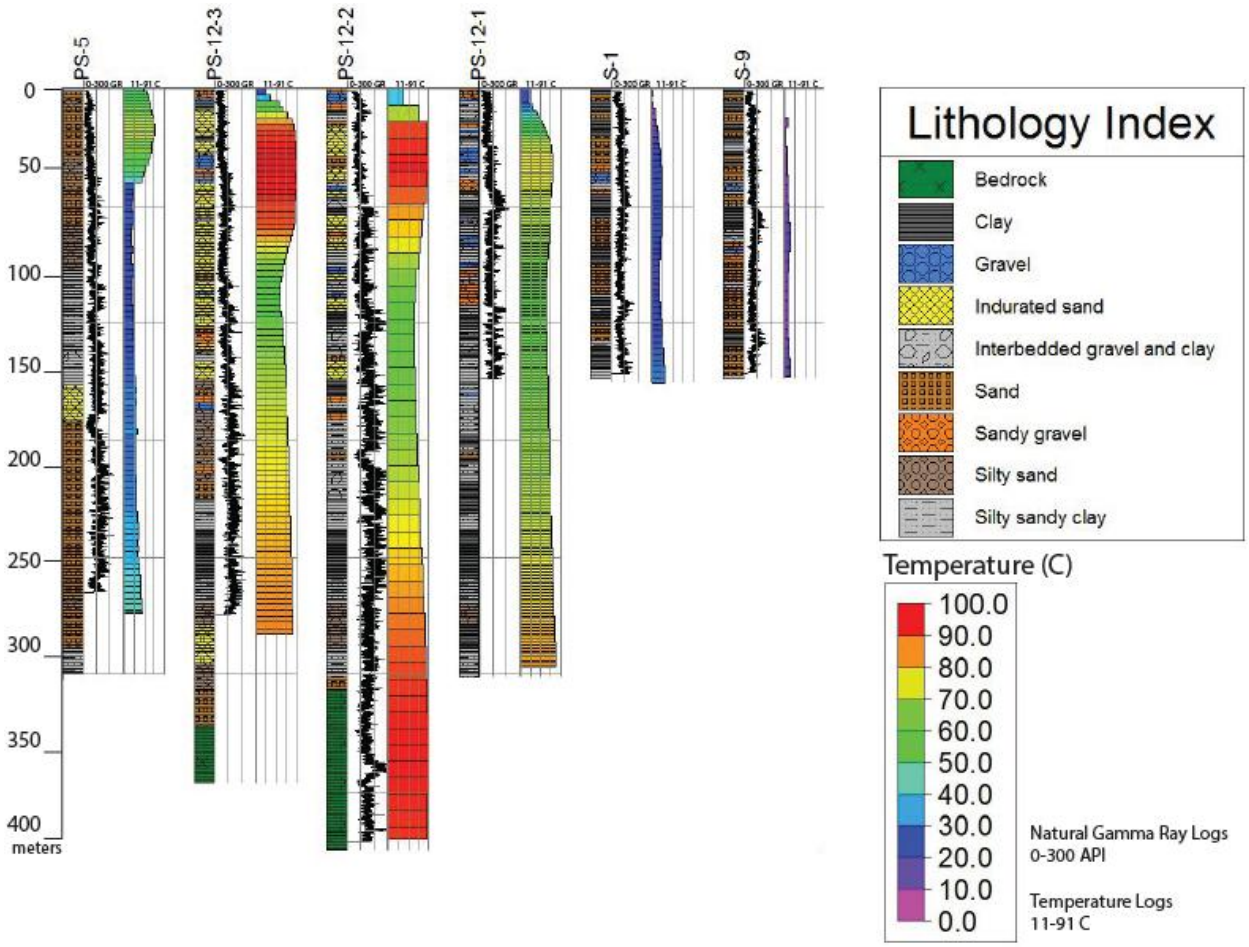

Figure 5. Lithologic, natural gamma ray, and temperature logs of several wells. Natural gamma ray is measured from 0-300 API and temperature is plotted from a minimum to maximum observed temperatures 11-91°C.

In Figure 5, lithology, gamma ray, and temperature logs for several wells are correlated by depth with equidistant spacing. The construction of the lithologic logs was guided by correlations of similar gamma ray peaks. Sticking issues with logging PS-5, PS-12-3, and PS-12-1 prevented from more complete gamma ray curves. Gamma ray counts are highest and most definitive in clay at 175-300 API. Low counts from 0-100 API are observed for the gravels and mixed sands. Indurated zones are typically within 100-200 API. A correlated trend of peaks at 75 m and again at 125 m in PS-12-2 through S-9 suggests significant clay layers with minor offsets or differential compaction between S-1 and S-9. The thick clay interval at 200-275 m is apparent in PS-12-2 marked by a low to 100 API at 200 m and peaks to 300 API below.

The temperature logs in Figure 5 were plotted as 11-91°C from lowest to highest observed temperatures. The high temperatures in the interpreted outflow aquifer, that peaks at 91°C at ~50 m, correlates well with layers of indurated sand and interbedded gravels. The indurated sand must have sufficient porosity and permeability to serve as a reservoir for geothermal fluids without excessive heat loss to colder groundwater. Internal fractures or hydrothermal-induced secondary porosity may provide the required storage capacity and fluid flow permeability. The outflow is capped by a thin clay layer that is present in each well (Fig. 5). The clay layer of 200-275 m has increasing temperatures below to the basement surface, potentially capping a deeper geothermal reservoir. Below the clay is a moderately-sorted sand interval to the basement surface separated by a 25 m thick clay layer at 300 m depth that appears in every deep well except PS-12-3 where induration has occurred. Cementation from upward migrating supersaturated fluids could have caused induration in the well-sorted sands where permeability was highest.

MAGNETOTELLURIC (MT) SURVEY

The locations of the MT stations at Pilgrim Hot Springs were determined by maximum spacing for best resolution and accessibility constraints. In total, 59 stations recorded at 0.001-10000 Hz range overnight with an average distance of 100 m distance apart with a remote station 5 km SE from the site (Figure 1). Data processing and recording equipment was provided by FUGRO Electric Magnetics Italy Srl.

The 200 m MT map shows an area of very low resistivity between PS-12-1, PS-12-2, and PS-12-3. A distinct boundary is seen where the resistivity increases rapidly from the west to the south. The boundary crosses at PS-5 at this depth where temperatures of 30°C are measured. The boundary could be the result of groundwater flowing into the system. At 500 m depth, the MT map is imaging the basement and shows a low resistive zone under all wells south of PS-12-1. The zone is centered under PS-5 and disappears by 750 m depth. No major compositional changes in the mica schist bedrock are known as no wells have reached this depth. However, the possibility exists that the conductor in the basement could be graphitic schist which occurs in the nearby Kigluaik Mountains. The low resistive zone could also be a conductive structure not observed on the surface such as a fault or fractures associated with the upflow of geothermal fluids that are feeding into the hot springs.

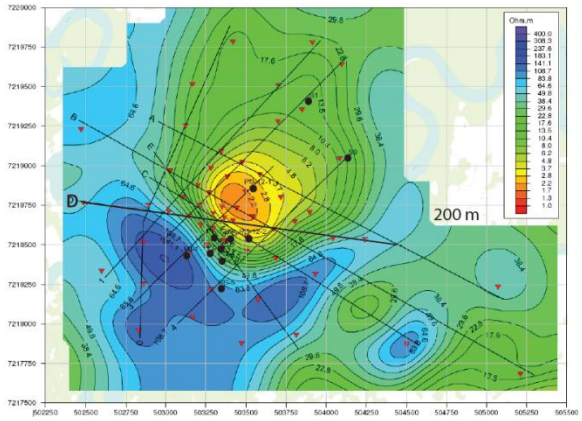

Figure 6. 200 meter depth plan map of the MT survey with resistivity values are 0-400 ohm-m.

MT Profile D (Fig. 8) shows a large, very low resistivity pattern (<1 ohm-m) from 150 m to 400 m which extends into the top of the basement and is sharply bounded by increasingly resistive zones on the west (left) and east (right). Areas of high resistivity values are interpreted as permafrost (0-100 m) and cold regional groundwater influx. The <0.5 ohm-m zone matches very closely to the modeled stratigraphy of the thick clays from 200-275 m in wells PS-12-2 and PS-12-3. The clay interval is assumed to be a smectite or a mixed layer clay and resembles a low permeability, low resistivity clay cap to a geothermal reservoir underneath (Cumming, 2009). This correlates with the top of the low resistivity zone seen in the 200 m MT map (Fig. 6). A shallow, flat, low resistivity layer of 2.4 ohm-m at 50 m depth aligns with the indurated zone in all three wells, notably PS-12-3 and PS-1.

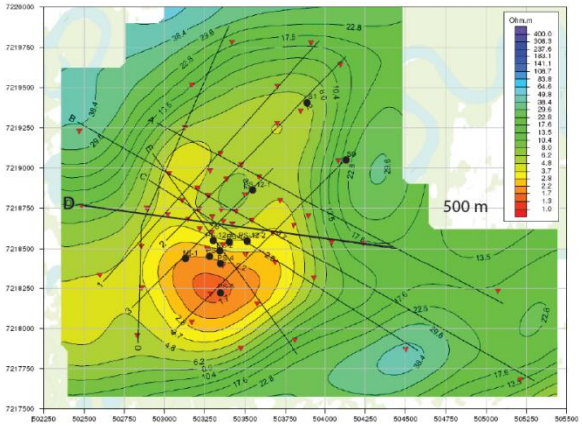

Figure 7. 500 meter depth plan map of the MT survey with resistivity values are 0-400 ohm-m.

CONCEPTUAL MODEL

The stratigraphy as determined from lithological correlations has been used to develop a conceptual model of the geothermal system. Low and high permeability sediments compliment temperature logs that have been used to characterize geothermal fluid flow. A simple conceptual model of the MT cross-section and isotherms is shown in Figure 9. Groundwater flow as drawn is flowing from the resistive western and eastern boundaries into the system where it eventually mixes with the outflow. Realistically, the flow is generally directed into the cross-section and continues to the north towards the

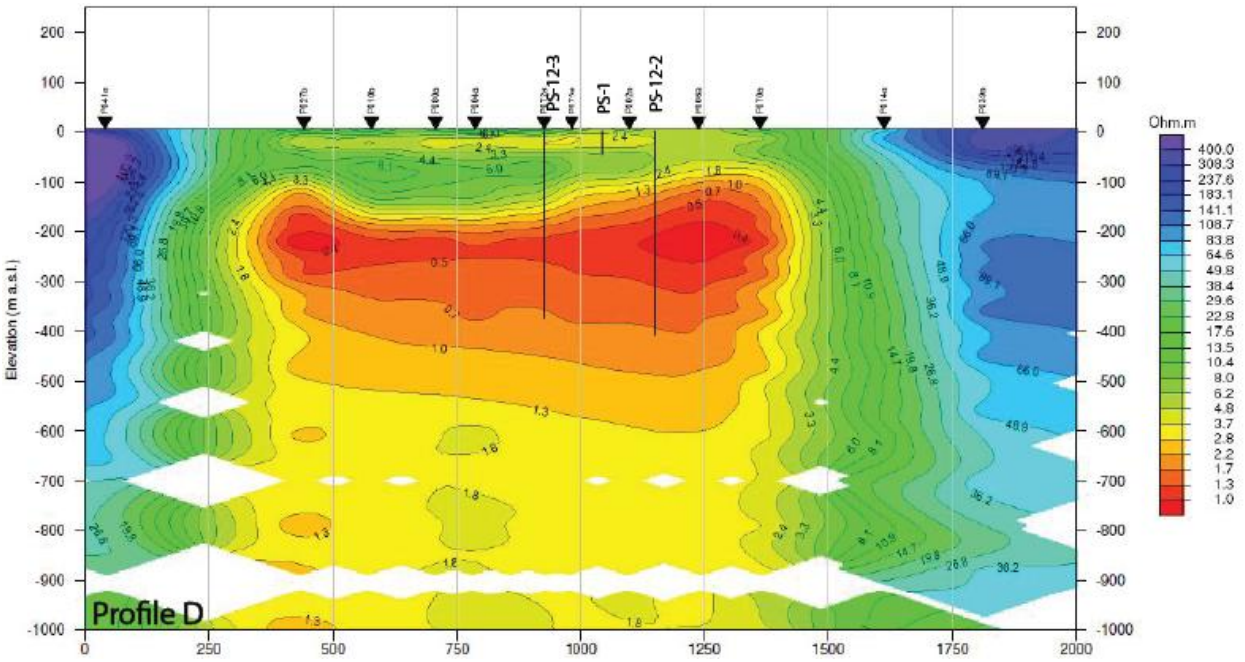

Figure 8. W-E Profile D cross-section from the MT survey (line plotted on Figure 6 & 7). Resistivity values are 0-400 ohm-m.

Pilgrim River. The thermally-buoyant outflow emanates out from the top of the 90°C plume with a stronger flow to the west and southwest above the influx. A small convection cycle may feed into the influx where the colder outflow settles on the margins of the system and mixes with the meteoric water. Isotherm placement is based on the distribution of temperatures from the wells. The tightly-spaced isotherms of 90-60°C indicate low permeability correlating to clay layers and indurated sediments (Cumming, 2009). The upflow of the 90°C geothermal fluids is a vertical conduit from basement to outflow and is constrained by the low permeability indurated sediments. Similarly, the close 80-30°C isotherms indicate the top of the clay cap of the geothermal reservoir. A deeper heat source of 100+°C has been placed under the PS-12-2, although the exact depth and location is hypothetical and only corresponds with the dip of the low resistive zone into the bedrock.

CONCLUSIONS

At Pilgrim Hot Springs the geothermal system is comprised of Quaternary sediments up to 320 m depth that overlie faulted mica-schist basement. Based on temperature, geophysical logs, MT survey, and lithologic data, the system can be subdivided into a shallow outflow aquifer and a deeper reservoir beneath a clay cap connected by a very narrow conduit of 90°C upflow. Temperature curves increase to 91°C at 25-50 m with a reversal at 30-100 m. The peak in temperature is the result of the outflow of geothermal fluids and the increasing temperature gradient is the heating of the deeper geothermal reservoir. The outflow direction is mostly concentrated to southwest. All wells show an increasing temperature gradient below the reversal of different rates. The temperature gradients suggest the upflow to be located between PS-12-1, PS-12-2, and PS-12-3. Stratigraphic correlations based upon well log data indicate several clay layers throughout the section with a dominant clay horizon at 200-275 m depth. Induration in the sediments is mostly concentrated between wells PS-4 and PS-12-3 and occurs from the shallow to near basement surface. The MT data matches closely to the modeled stratigraphy where thick clays from 200-275 m in wells PS-12-1, PS-12-2, and PS-12-3 correlate to the <0.5 ohm-m zone in the MT cross-section and appears in the 200 m depth map.

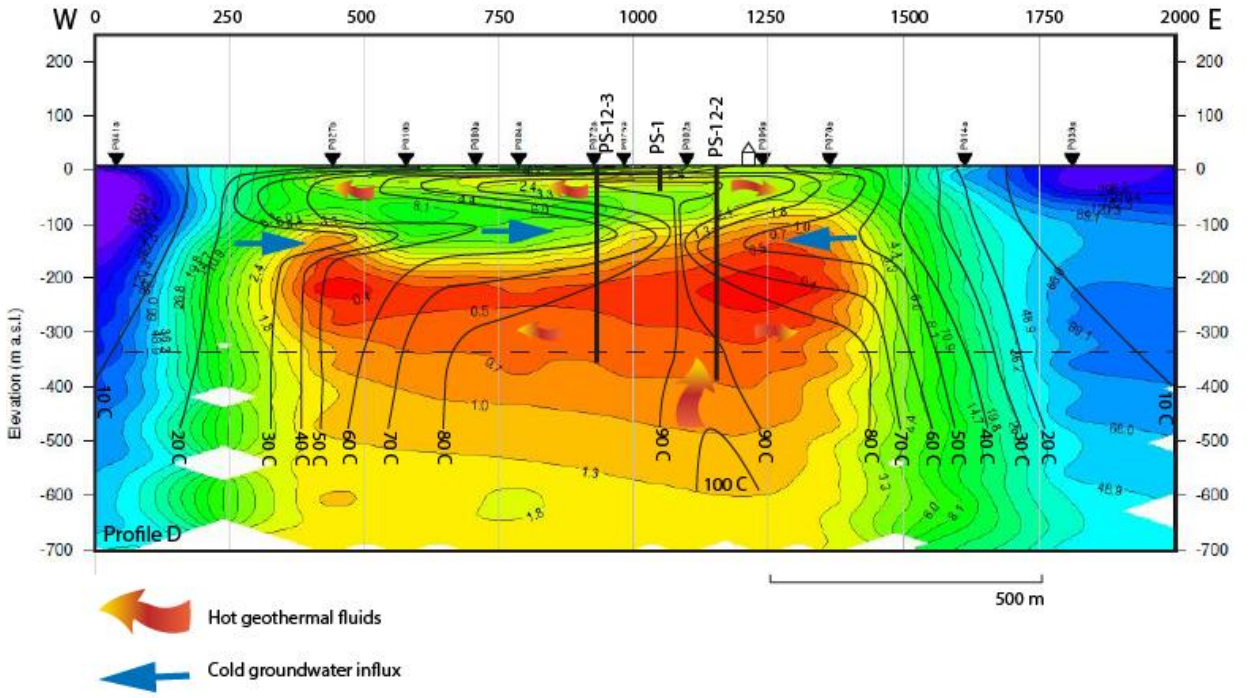

Figure 9. Simple conceptual model cross-section utilizing the W-E Profile D of the MT survey. Isotherms are plotted from 10-100°C with hot fluid and cold fluid arrows to indicate direction of flow. Bedrock-sediment contact has been dashed to indicate approximate extent.

The conceptual model proposes a shallow outflow aquifer in the indurated sediments with a thin clay cap at 50 m depth. The upflow has been placed between PS-12-2 and PS-12-3, although it is very narrow (<50 m) and the exact location is uncertain. The upflow also correlates well with the indurated zone possibly due to the porosity and permeability of the cemented sand which acts as a reservoir for geothermal fluids and can transmit fluid with less heat loss than unconsolidated sand. The clay interval at 200-275 m depth seen in the stratigraphic cross-section and MT survey is assumed to be a smectite or mixed layer clay. This interpretation is based upon its low resistivity values and resemblance to a low permeability, low resistivity clay cap.

Our conceptual model is restricted by our current limited understanding of the structural geology controlling fluid flow under Pilgrim Hot Springs. The placement and orientation of any fault-related offsets between wells at depth is difficult to ascertain as surface expression at the site is muted by swamp in warm months and snow in colder months. In Figure 2, the geologic map has a major ~N-S directed fault projected across the basin that transects the western edge of the thawed ground at Pilgrim. The fault is placed here due to a ~1 m terrace that runs roughly in the same direction. The terrace, however, could be the result of frost-heaving where frozen soils expand, causing an uplift in the immediate subsurface, as it forms an arc around the thawed ground anomaly (Fig. 1).

Potential production from this system is limited to where sufficient permeability exists in connection to the upflow. The silty sands beneath the clay layer at ~300 m close to PS-12-2 could have a high enough temperature and flow to be a feasible target for a large diameter production well.

The conceptual model will be complimented by the reservoir model, presented by Arvind Chittambakkam et al in this publication, which will evaluate the temperature and fluid flow conditions at Pilgrim Hot Springs for the purposes of testing the total energy flux estimation and deeper reservoir

location. The stratigraphy presented in this conceptual geologic model has been incorporated into the reservoir model to provide permeability calculations for a more effective fluid flow model.

REFERENCES

Amato, J. M., & Miller, E. L. (2004) "Geologic map and summary of the evolution of the Kigluaik Mountains gneiss dome, Seward Peninsula, Alaska," *Geological Society of America Special Papers*, v. 380, p. 295-306.

Cumming, W. (2009) "Geothermal resource conceptual models using surface exploration data," Proceedings, *Thirty-Fourth Workshop on Geothermal Reservoir Engineering*, Stanford University, SGP-TR-18.

Daanen, Ronald P., Chittambakkam, Arvind, Haselwimmer, Christian, Prakash, Anupma, Mager, Markus, Holdmann, Gwen (2012) "Use of COMSOL Multiphysics to Develop a Shallow Preliminary Conceptual Model for Geothermal Exploration at Pilgrim Hot Springs, Alaska," *Geothermal Resource Council Transactions*, v. 36, p. 631-635.

Haselwimmer, C., Prakash, A., Holdmann, G. (2011) "Geothermal Exploration in Pilgrim, Alaska Using Airborne Thermal Infrared Remote Sensing," *Geothermal Resource Council*, 35th Annual Meeting, Oct 23-26, San Diego, California.

Lofgren, B.E. (1983) "Results of Drilling, Testing and Resource Confirmation -Geothermal Energy Development at Pilgrim Springs, Alaska: Unpublished report of Alaska," Woodward-Clyde Consultants to Alaska Division of Energy and Power Development, *Technical Report*.

Ruppert, N. A. (2008) "Stress map for Alaska from earthquake focal mechanisms," in *Active Tectonics and Seismic Potential of Alaska*, Geophys. Monogr. Ser., vol. 179, edited by J. T. Freymueller et al., pp. 351–367.

Till, Alison B., Dumoulin, J. A., Werdon, M. B. Bleick, H. A. (2011) "Bedrock Geologic Map of the Seward Peninsula, Alaska, and Accompanying Conodont Data," *U.S. Department of the Interior*, U. S. Geological Survey.

Turner, D. L., Forbes, R. B. (1980) "A Geological and Geophysical Study of the Geothermal Energy Potential of Pilgrim Springs, Alaska," Geophysical Institute, University of Alaska, UAG R-271, *Technical Report*.

Turner, D.L., Swanson, S., Forbes, R. B., Maynard, D. (1979) "Geologic map of the Bendeleben A-6 and eastern part of the Teller A-1 quadrangles, Alaska," *Technical Report*.

Authors continued:

[2]Geophysical Institute, University of Alaska Fairbanks, Fairbanks, AK, USA; aprakash@alaska.edu

[3]Water and Environmental Research Center, University of Alaska Fairbanks, Fairbanks, AK, USA; rdaanen@alaska.edu

[4]Geophysical Institute, Univeristy of Alaska Fairbanks, P.O. Box 750421, Fairbanks, AK, 99775, USA; chha@gi.alaska.edu

[5]Department of Geology & Geophysics, University of Alaska Fairbanks, Fairbanks, AK, USA; mtwhalen@alaska.edu

[6]Consultant, Reno, NV, USA; dickbenoit@hotmail.com

[7]Cumming Geoscience, 4728 Shade Tree Lane, Santa Rosa, CA 95405-7841, USA; wcumming@wcumming.com

[8]USGS Central Region Research Drilling Program, Denver, CO, USA; aclark@usgs.gov

[9]Alaska Center for Energy and Power, University of Alaska Fairbanks, Fairbanks, AK, USA; markus.mager@alaska.edu

[10]Alaska Center for Energy and Power, University of Alaska Fairbanks, Fairbanks, AK, USA; gwen.holdmann@alaska.edu